Simulative investigation of a bidirectional 10×100Gbps ring-shaped PON using integrated OFDM-OCDMA scheme over hybrid SMF-FSO-VLC links

VIVEK ARYA[1,*], TAPSI NAGPAL[2], BRAJESH KUMAR SHARMA[3], SHIPRA SHUKLA[4]
[1]*Phonics University Roorkee-247667, Uttarakhand, India*
[2] *IT Department New Delhi Institute of Management, New Delhi, India*
[3] *Padampat Singhania University, Udaipur, India*
[4]*School of Computing Science, CSE Galgotias University, Greater Noida, India*

A hybrid orthogonal frequency division multiplexing and optical code division multiple access techniques based bidirectional passive optical local area network (POLAN) system is designed and investigated for hospital applications. The results reveal reliable fiber, free-space and visible light communication range of 50km, 100m and 10-20m, respectively, at 10×100Gbps data rate under clear air climate and weak turbulence scenarios. Also, the system offers maximum -8.5dBm received power, 1dB power penalty and it can serve upto 300 end nodes. Comparative literature reveals its design superiority over other existing designs in terms of design performance.

(Received May 29, 2025; accepted April 6, 2026)

Keywords: 2D-MFRS, POLAN, PON, VLC, FSO

1. Introduction

Passive optical networks (PONs) are trending towards a promising solution to permit a high traffic rate and long-reach transmission architecture handling multiple end units [1]. Again, the second-generation next generation PON stage 2 (NG-PON2) is proposed as adjunct to next generation PON stage 1 (NG-PON1) to sustain higher bandwidth as well as throughput, primarily because of rapid expansion of internet service. NG-PON2 basics time and wavelength division multiplexing PON (TWDM-PON) with 64 splitting ratio can supports at least 40Gbps traffic rate over 60km reach at low cost to assist mobile, business, smart cities and healthcare applications [2,3]. But due to intensity modulation, low receiver sensitivity as well as direct detection PONs still has restricted transmission range in ODNs. To conquer these issues, optical networks require coherent transmission which can operate over long-reach having leading receiver sensitivity as well as spectrally effective higher-order modulation together with phase-polarization diversity. In particular, TWDM-PONs using orthogonal frequency division multiplexing (OFDM) can provide an efficient and flexible multiple-access function [1].

Again, indoor or short range based OFDM-visible light communication (VLC) systems comprising light emitting diode (LED) are mostly used in hybrid wired-wireless networks as a backup wireless connection and a point-to-point last-mile access in various applications requiring no electromagnetic interference. Various systems of OFDM-VLC have been reported for effective transmission over long-reach. In [4], an OFDM-VLC design at VLC range of 0.5m for 157.5Mbps transmission rate has been reported. An another work [5], OFDM-VLC system over 1m VLC range at 682Gbps information rate has been reported. Also, in [6] as well as [7], a hybrid OFDM-VLC architecture at VLC range of 3.5m with 30Mbps and 3.63Gbps throughput respectively, has been presented. In [8], OFDM-VLC system over 2m VLC range at 6.14Mbps transmission rate has been presented. Besides this, a hybrid OFDM wavelength division multiplexing (WDM) with VLC system at 1.87Gbps transmission rate over 0.8m VLC communication has been demonstrated in [9]. In [10], a multi-channel VLC system for uplink transmission at 682Mbps using time division multiple access has been realized.

As the integration of PON enables numerous splitting points by permitting several end users to access the scalable architecture via optical line terminal (OLT). Nevertheless, various topologies have been described for PONs to compose credible communication like tree, bus, star, ring and mesh. Recent works focus on exploring as well as advantaging from reliable topology hybrid fiber-wireless system to develop reliability in high-speed communication. Wheel based hybrid PON with free-space optics (FSO) and VLC is a new topology than ring or star but provides improvised facilities for network protection under distinct disaster scenario over others. Also, it provides low cost, high speed and long-reach communication [11,12]. In literature, several topologies have been reported in the past that are capable to fulfill end users demands. A tree-based PON incorportaing self-restroable apparatus has been proposed as well as investigated in [13]. Again in, [14–17], the proposed OFDM systems illustrate limited wireless (≤100m) and wired transmission range (≤60km) without considering VLC link at limited data rate.

1.1. Problem statements

- The comprehensive review depicts that previous studies are generally focused on low traffic rate and worse spectral efficiency.
- The researchers mainly focused on either individual or combination of two multiplexing technique rather than the integration of four multiplexing schemes viz. TWDM, WDM, optical code division multiple access (OCDMA) and OFDM based on wheel topology using integrated PON/FSO link with VLC communication for hospital scenario.
- Till now, a wheel-based hybrid PON/FSO/VLC healthcare system offering the primary hospital services like localization of medical staff or patient, medical video conferencing or treatment, intelligent controllability and indoor navigation is not realized.

1.2. Motivation and contributions

From last few years, hybrid fiber-wireless networks due to their long-distance communication and high capacity have been utilized as the primary communication technology to facilitate network traffic, especially for transport, smart building, ground to satellite, underwater, healthcare and fifth generation-based communication networks. Regrettably, these networks are critically hindered by immense failures caused by malicious human activities, natural disasters as well as weather-related disruptions. Thus, there is a need work on these scenarios especially healthcare systems to enhance the disaster resilience of network against the several classes of disaster events.

In this work, wheel basics POLAN healthcare system using wheel topology under distinct atmospheric scenario is realized and investigated for disaster preparedness.

The major contributions of this work are:

- However, integrated PON/FSO or integrated PON/VLC architectures have been studied over the past 10 years, but NGPON3 basics hybrid OCDMA, OFDM, WDM techniques for healthcare applications is reported first ever in this work. For this, a novel wheel based passive optical local area network (POLAN) healthcare system for disaster preparedness. NG-PON based four multiplexing techniques i.e. TWDM, OFDM, OCDMA and WDM using two-dimensional modified fixed right shifting (2D-MFRS) OCDMA code are combined to realize a real-time intelligent healthcare system. Bedsides this, various medical services are provided via bidirectional hybrid fiber-FSO with VLC links at symmetric 40Gbps transmission rate serving various end users.
- Proactive protection architecture for hybrid optical wired-wireless networks against failures arises from unpredictable disasters (weather-induced disruptions) is investigated. It is shown that the proposed architecture allows high bandwidth, high speed, long-reach, flexible, reliable, easy upgradeable, supporting large number of users, low cost, mobile, secure and human friendly communication concerning wired-wireless channel impairments.
- An OCDMA code, a 2D-MFRS code for secure transmission and for medical data protection in healthcare networks is also employed. The results depict an excellent design of healthcare system capable of supporting large number of users through hybrid fiber/FSO/VLC links, ideally suitable for long reach, mobile, flexible and cost effective wired-wireless systems for disaster preparedness.
- For proposed work validation, the performance of design is compared to existing ones.

This work is structured as: Proposed architecture considering fiber, VLC, and FSO links disturbances is presented in Section 2. Mathematical analysis and evaluated results with discussion are shown in Section 3. Conclusion remarks with future scope are exhibited in Section 4.

2. Proposed design

Fig. 1 describes the conceptual diagram of wheel-hybrid PON/FSO/VLC healthcare system. In the design, OLT (hospital management) is positioned in the mid of bidirectional hybrid fiber-FSO ring connected directly to ‘n’ number of remote nodes (RNs) which are again linked via bidirectional hybrid fiber-VLC links to ‘n’ number of optical network units (ONUs) as end nodes to across the ring [11].

Here, ONUs represent patient room, medical expert (doctors/nurses), rural area healthcare centre, multi-speciality hospital, video conferencing, telemedicine, medical robot and many more commented users/subscribers and devices. Distinct wavelengths λ_1 - λ_n are assigned for downstream (DS) and upstream (US) transmission in all remote nodes (RNs) as well as ONUs. OLT facilitates inter-node communication at RN, identification, along with control. Also, the broadcasting, completion, regeneration, and rebroadcasting of wavelengths for OLT path are carried out either anti-/clockwise via bidirectional ring at each RN in the wheel topology. Additionally, the OLT in this wheel-based architecture is fixed with an ‘n’-secure number of OCDM code-enabled transmitters (Txs) and receivers (Rxs) [11].

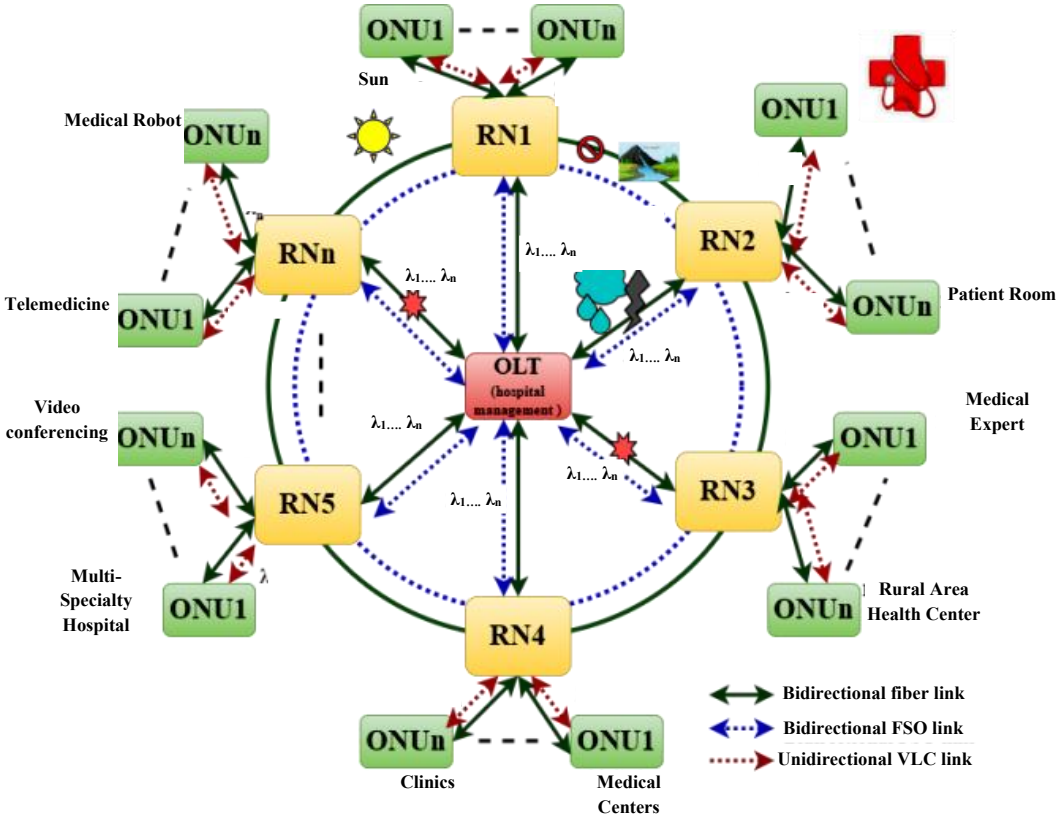

Fig. 1. Concept of the proposed wheel based POLAN healthcare system

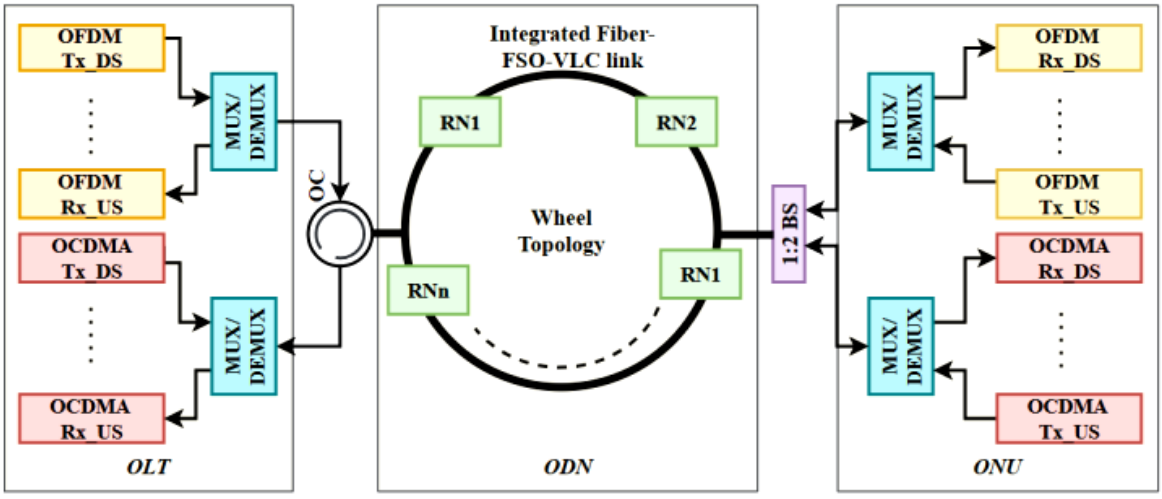

(a)

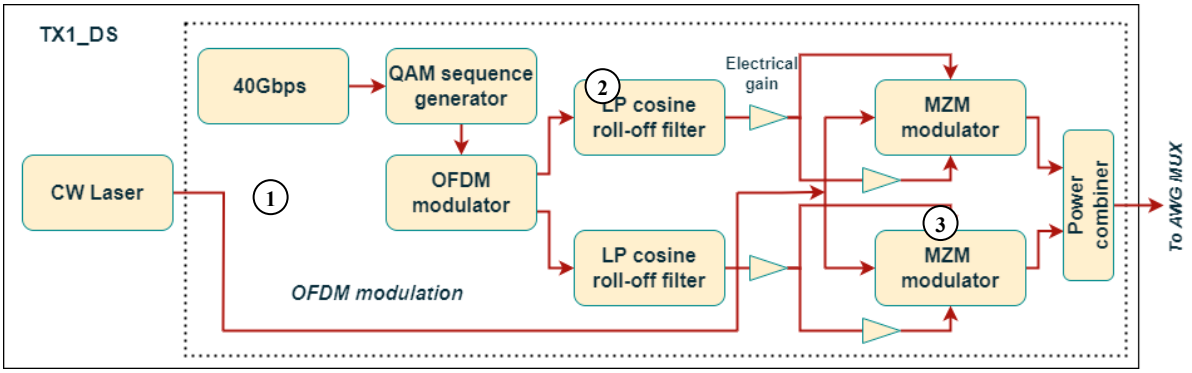

(b)

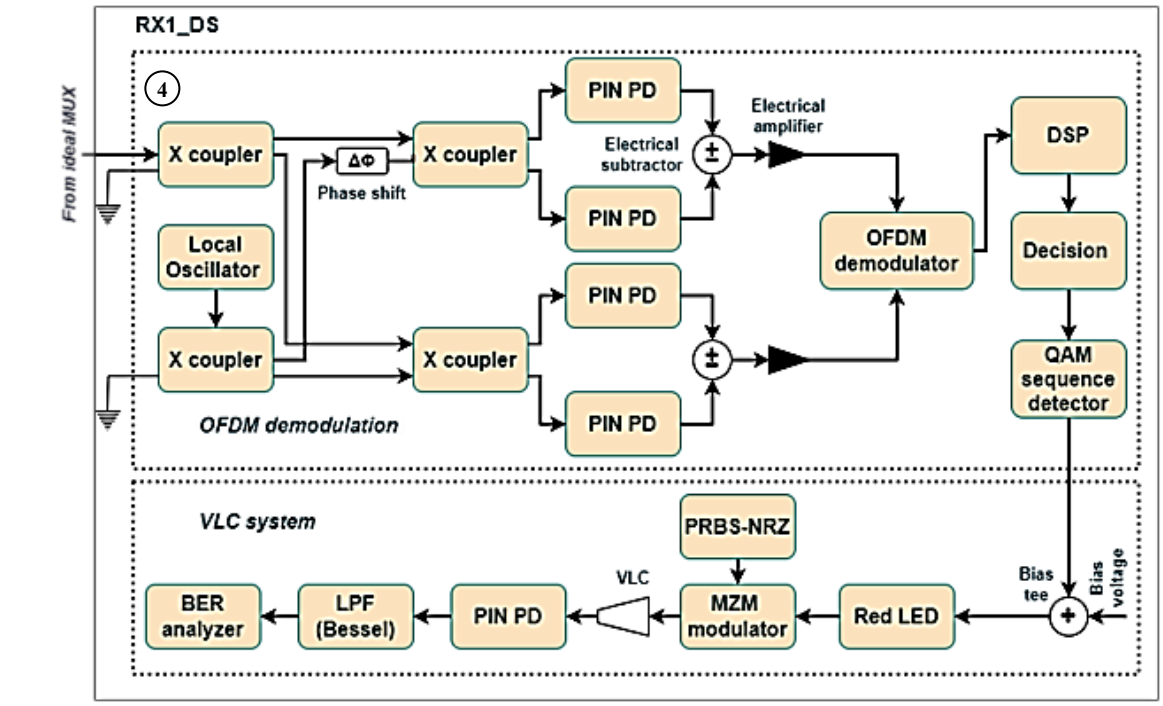
RX1_DS
4
From ideal MUX
X coupler
ΔΦ
Phase shift
X coupler
PIN PD
Electrical subtractor
PIN PD
Electrical amplifier
DSP
Local Oscillator
OFDM demodulator
Decision
X coupler
X coupler
PIN PD
QAM sequence detector
OFDM demodulation
PIN PD
VLC system
PRBS-NRZ
VLC
Bias tee
Bias voltage
BER analyzer
LPF (Bessel)
PIN PD
MZM modulator
Red LED

(c)

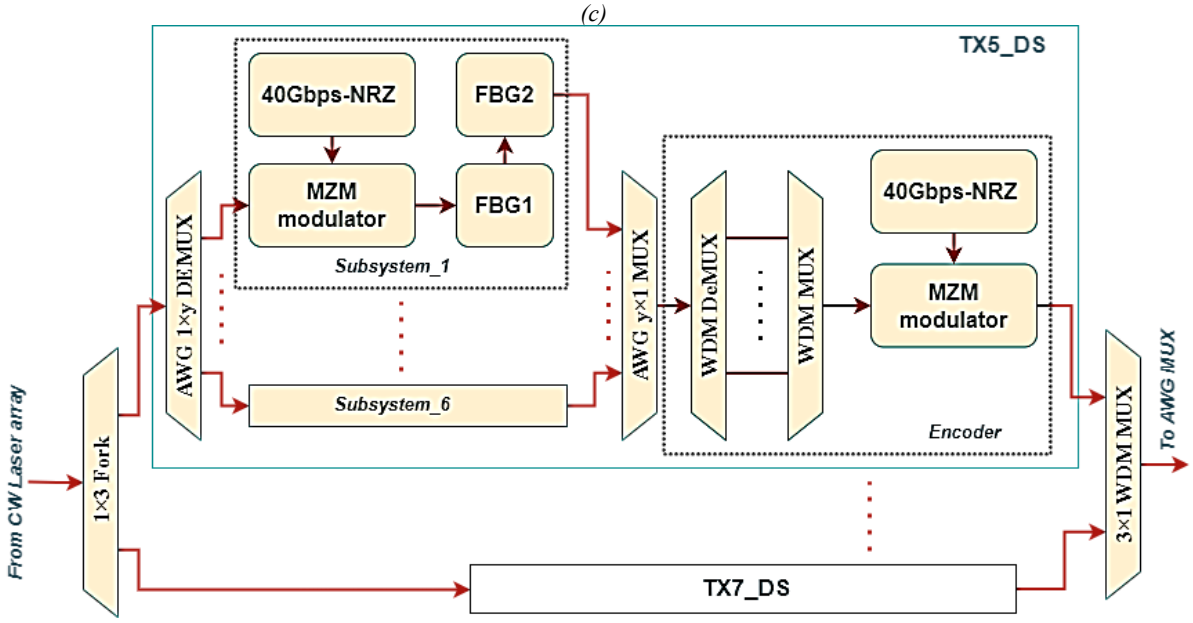
TX5_DS
40Gbps-NRZ
FBG2
MZM modulator
FBG1
Subsystem_1
Subsystem_6
AWG 1×y DEMUX
AWG y×1 MUX
WDM DeMUX
WDM MUX
40Gbps-NRZ
MZM modulator
Encoder
From CW Laser array
1×3 Fork
3×1 WDM MUX
To AWG MUX
TX7_DS

(d)

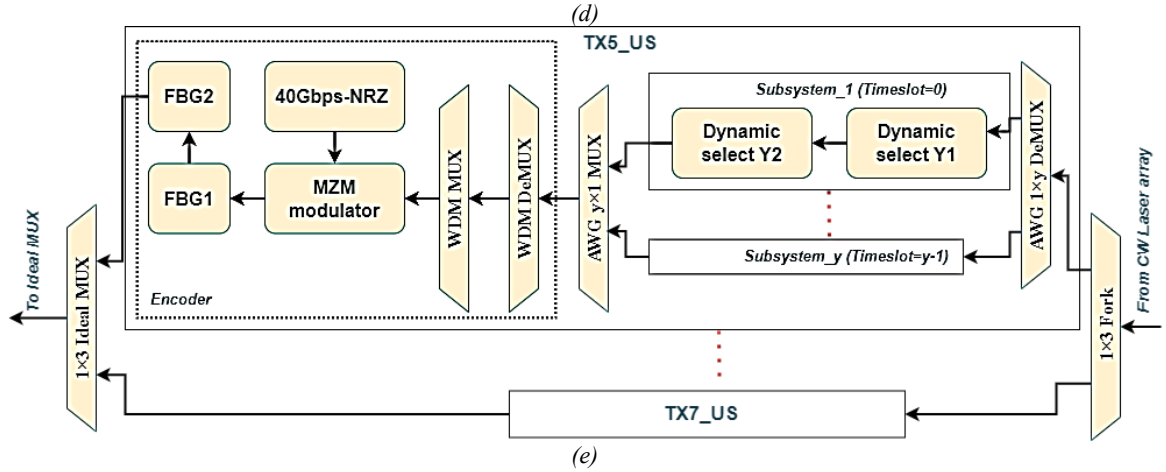
TX5_US
FBG2
40Gbps-NRZ
Subsystem_1 (Timeslot=0)
Dynamic select Y2
Dynamic select Y1
FBG1
MZM modulator
WDM MUX
WDM DeMUX
AWG y×1 MUX
AWG 1×y DeMUX
Subsystem_y (Timeslot=y-1)
Encoder
To Ideal MUX
1×3 Ideal MUX
From CW Laser array
1×3 Fork
TX7_US

(e)

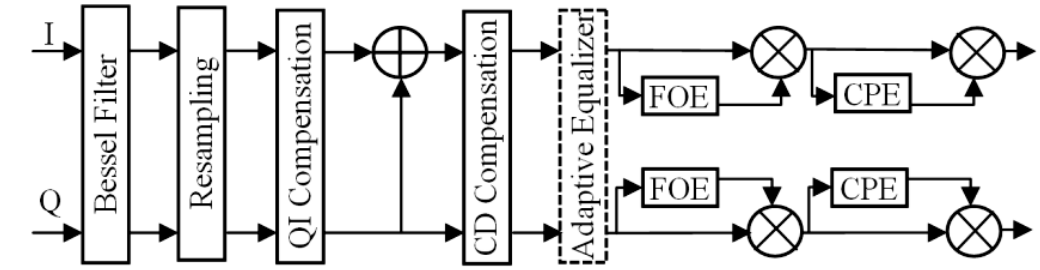

QI: Quadrature Imbalance, CD: Chromatic dispersion,
FOE: Frequency offset estimation, CPE: Carrier phase estimation

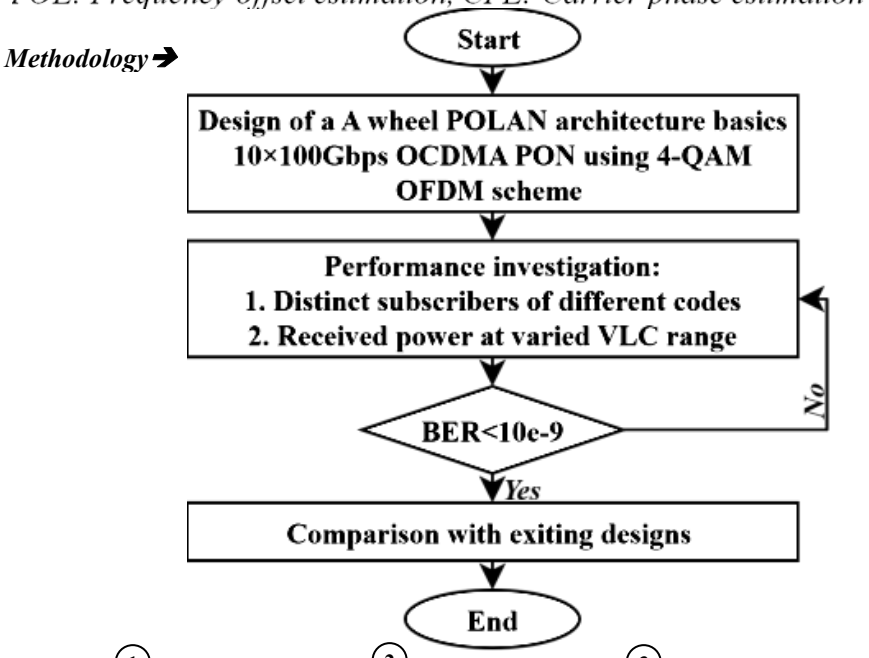

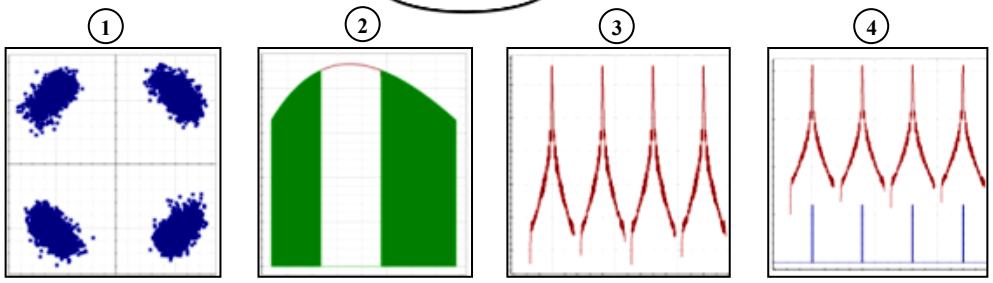

(f)

Fig. 2. (a) Conceptual diagram of wheel-POLAN system, block diagram of (b) DS Tx section, (c) DS Rx section; hybrid OCDMA-WDM using 2D-MFRS code (d) DS Tx section, (e) US Tx section, and (f) DSP module; insets: observed spectra along with methodology (colour online)

As depicted in Fig. 2(a), the DS and UP traffic at end nodes is handled by each RN connected to various ONUs using different wavelengths at each Tx/Rx over hybrid fiber-VLC links. In this design, the fiber and FSO links capacity will be used under link failure scenario under various disaster conditions. The communication networks for healthcare services are the crucial infrastructure as well as backbone of the modern e-Health systems. In contrast, regional failures mean natural disasters along with cost-effective system design, pose a significant threat to its quality of service and capacity. Thus, it is prominent to purpose a communication network which is resilient sufficient to withstand disasters. To realize the healthcare services operating at long-haul high-speed data transmission in disaster preparedness conditions, wheel architecture based POLAN system is designed.

As depicted in Fig. 2(b), an integrated TWDM-OFDM PON, both OLT and ONUs comprise four pairs of transmitters and receivers. Here, 4- Quadrature Amplitude Modulation (QAM) *modulation* is incorporated with 32768 *number of samples* and 2.5×10^9 symbols/s *symbol rate* to design the system. Also, FFT size and symbol length of 128 with no cyclic prefix, is considered for the proposed 4-QAM OFDM based system [18].

Four downstream (1596, 1596.8, 1597.6 and 1598.4nm) and four upstream each at 10Gbps (1527, 1527.8, 1528.6 and 1529.4nm) wavelengths for TWDM-OFDM PON integrated strictly as per ITU-T 0.8nm channel spacing. At OLT side, in a single downstream transmitter

section random binary sequences are generated at 40Gbps transmission rate which are forward to 4-QAM sequence generator. Then, the output QAM signal is modulated utilizing an OFDM modulator comprising 512, 1024 and 64 subcarriers, fast Fourier transform points and cyclic prefix points respectively. In-phase (I) & quadrature (Q) signals generated are filtered via a couple of roll-off filters (roll-off factor=0.2 for low pass cosine) for I/Q components modulation. I/Q modulator includes an incoming continuous wave (CW) laser signal (linewidth=0.15MHz, input power=-6dBm), twice pairs of electrical gain after each filter, a pair of mach-Zehnder modulators (MZMs). A 2:1 power combiner is used to combined the incoming I/Q optical modulator outputs. Likewise, four DS TWDM-OFDM beams are multiplexed by 4:1 array waveguide grading (AWG) MUX at different wavelengths and transmitted over fibre/FSO hybrid link [19].

As depicted in Fig. 2(c) at ONU side, for DS signal reception, incoming de-multiplexed signal is sent to two X couplers pairs (coupling=0.5) along in combination with a local oscillator & 90^0 phase shift components to receive coherent orthogonal signals. Then signals are passed to two sets of PIN photodetectors (PDs) for coherent detection which is followed by the pairs of electrical subtractor and electrical amplifier (gain=20dB). To fix fiber nonlinearities & FSO noise, the demodulated signals are forward to subsequent a *digital signal processing* (DSP) unit, a decision apparatus as well as a sequence decoder (4-QAM). To reconstruct the QAM symbols correctly at RX, the demodulator performance measures should meet with the Tx. To recover the Tx bit sequence, a QAM sequence detector helps to identify the binary sequences as well as de-mapped the electrical signal. Furthermore, to generate VLC signals at end of OFDM demodulator Rx section, incoming electrical signal is integrated with DC bias signal having voltage of 4V using a bias tee which is utilized to drive a red LED (quantum efficiency=65%, wavelength=625nm, bandwidth=1GHz). A VLC channel is used to transmit generated LED signal after re-modulation through MZM modulator at 40Gbps pseudo random bit sequence-non return to zero (PRBS-NRZ) signal. Ultimately, VLC signal is identified via PIN PD which is accompanied by a filter and a bit error rate (BER) device [19].

Moreover, UP Tx section of hybrid TWDM-OFDM/VLC PON incorporates four input signals (1527, 1527.8, 1528.6 and 1529.4nm) generated by four laser diodes as depicted in Fig. 2(d). Each input signals is passed through time switch having two consecutive dynamics select Y to generate the US signals at specific time and then forwarded to a OFDM modulator. These signals are demodulated at OLT side via OFDM demodulator. Buffer selector is incorporated to select the final iteration of received signals.

Fig. 2(e) depicts DS Tx section of hybrid WDM-OCDM using 2D-MFRS code, where both OLT and ONU section incorporates thrice Tx/Rx pairs for three coded users. For DS and US Tx section of WDM-OCDM, six CW lasers produce six DS and six US wavelengths at 10Gbps (1575-1579nm and 1527-1531.8nm) are used at 10Gbps per wavelength. DS wavelengths are fed into a n:1 AWG MUX (n=6) followed by a 1×3 Fork for three DS Txs. Each Tx section incorporates, 1×y AWG DEMUX (demultiplexer) having y=6 indicating six input signals. The outputs from AWG DEMUX are transferred to a Subsystem_1 to Subsystem_6 where a single Subsystem consists of a PRBS-NRZ bit sequence which is modulated by a MZM modulator. The modulated signal is passed to two consecutive fibre Bragg grading (FBG) i.e. FBG1 and FBG2. A y×1 AWG MUX is used to multiplexed the incoming signals from Subsystems to forward these signals to encoder. Each encoder incorporates a 1×6 WDM DEMUX followed by a 6×1 WDM MUX which transferred the data into MZM modulator to be modulated with PRBS-NRZ random sequences throughput. Then the coded multiplexed signals are multiplexed by a 3×1 WDM MUX to transmit the data over bidirectional hybrid fiber-FSO links. At ONUs side, reverse process is done to decode the signals using decoder followed by PD, filter and BER analyzer.

Here, Bessel filter incorporates 8×samples/bit of samples/symbol and 0.75×symbol rate bandwidth. After this resampling is achieved at a rate of four samples/symbol followed by QI compensation to minimise the phase and amplitude imbalances within QI signals. CD compensation helps to eliminate CD as well as fibre nonlinearity through Back-Propagation algorithm. Also, an adaptive equalizer executes a butterfly structure for de-multiplexing the received signal polarization. Meanwhile, FOE is incorporated to eliminate the phase & frequency mismatch between Tx and Rx. CPE is utilized to offer better output w.r.t. distances and bit rates. Thus, input signal at DSP unit is expressed as [20]:

$$Y(k) = C(k).e^{j(2\pi \triangle fkT+\varphi_k)} + N(k) \quad (1)$$

where $C(k)$=data symbol, $\triangle f$ = carrier frequency offset, T=symbol period and φ_k= carrier phase, $N(k)$=zero-mean Gaussian random variable. $Y(k)$ in the fourth power can be expressed as [20]:

$$Y^4(k) = A.e^{4j(2\pi \triangle fkT+\varphi_k)} + E(k) \quad (2)$$

where A= constant amplitude, $E(k)$=noise with zero-mean. Also, frequency offset can be given as [20]:

$$Y^4(k) = \frac{1}{4} arg\{\max[|R(f)|]\} \quad (3)$$

where $R(f)$=frequency-domain correlation.

2.1. 2D-MFRS code properties

The code matrix for FRS code is shown as [21]:

$$FRS\ Matrix = \begin{bmatrix} 0 & \dots 0 & LNE_1 & FNE_1 \\ 0 \dots & LNE_2 & FNE_2 & 0 \\ 0 \dots & . & \dots 0 & \vdots \\ 0 \dots & . & \dots 0 & \vdots \\ 0 \dots & . & \dots 0 & \vdots \\ LNE_N & FNE_N & 0 & \dots 0 \end{bmatrix} \quad (4)$$

where $LNE_{1\ to\ N}$ and $FNE_{1\ to\ N}$ are the last non-zero as well as first non-zero elements considerably. 2D-MFRS it is constructed through utilizing FRS code sequences. 2D-MFRS code incorporates an $S \times L$ matrix, where S is code size and L is code length. Fig. 2(f) illustrates the DSP unit. Table 1 defines code design used in system and Table 2 depicts simulation parameters.

Table 1. 2D-MFRS code construction [21]

	$Q_1 = [0\ 0\ 0\ 0\ 0\ 1\ 0\ 1\ 1]$
$P_1^T \begin{bmatrix} 0 \\ 0 \\ 0 \\ 1 \\ 0 \\ 1 \\ 1 \end{bmatrix}$	$\begin{bmatrix} 0 & 0 & 0 & 0 & 0 & 0 & 0 & 0 & 0 \\ 0 & 0 & 0 & 0 & 0 & 0 & 0 & 0 & 0 \\ 0 & 0 & 0 & 0 & 0 & 0 & 0 & 0 & 0 \\ 0 & 0 & 0 & 0 & 0 & 1 & 0 & 1 & 1 \\ 0 & 0 & 0 & 0 & 0 & 0 & 0 & 0 & 0 \\ 0 & 0 & 0 & 0 & 0 & 1 & 0 & 1 & 1 \\ 0 & 0 & 0 & 0 & 0 & 1 & 0 & 1 & 1 \end{bmatrix}$

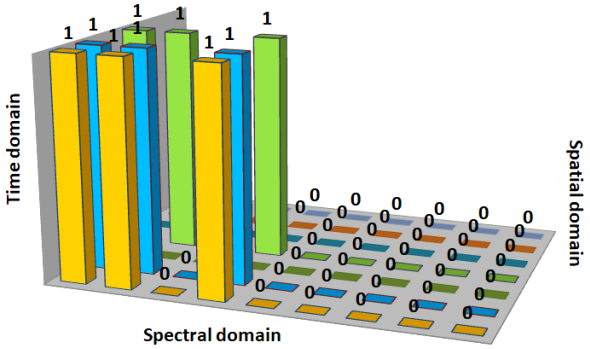

Fig. 3. 3D-view of 2D-MFRS code design (colour online)

Furthermore, as in the proposed architecture, seven ONUs are used per remote node (Fig. 2(a)). Thus, to enhance the ONUs per RN, 1:4 power splitter is used at RN followed by four number of 1:8 power splitters. Fig. 3 depicts 3D view of 2D-MFRS code view.

Table 2. Design parameters

Component	Parameters		Value	Unit
VLC	Range		10-20	m
	Tx/Rx aperture diameter		20	cm
	Attenuation		8	dB/km
FSO	Loss	Tx/Rx	1	dB
		Additional	1.5	dB
	Geometric loss		Yes	
	Scintillation	Gamma-Gamma (GG)	Yes	
	Optical beam divergence		2	mard
	Distance		100	m
	Attenuation	Clear air	0.2	dB/km
	Turbulence effects		10^{-17}	$m^{-2/3}$
	Wavelength		1550	nm
	Tx/Rx aperture diameter		20	cm
SMF	Dispersion slope		0.075	$ps.nm^{-2}.km^{-1}$
	Range		50	km
	Dispersion		16.75	$ps.nm^{-1}.km^{-1}$
	Temperature		300	K
	Attenuation		0.2	dB/km
BPS/PS	Type		1:2/8/32/64	
	Insertion loss		2	dB
	Return loss		50	
Circulator	Quantum Efficiency		0.65	%
	Bandwidth		4	dB
	Insertion loss		1	dB
MUX/ DEMUX	Filter type		Gaussian	
	Return loss		45	dB

Component	Parameters	Value	Unit
	Filter order	4	
	Insertion loss	3	dB
	Bandwidth	10	GHz
AWG	Bandwidth	0.16	nm
	Filter order	2	
	Filter type	Gaussian	
	Insertion loss	2	dB
	Channel spacing	0.8	nm

3. Results and discussion

Proposed architecture is simulated and analysed using OptiSystem and MATLAB. The following possibility are taken into account when measuring the system performance:

1. For both hybrid TWDM/OFDM PON (1596nm in DS and 1527nm in US) and hybrid WDM-OCDM systems (1575nm in DS and 1260nm in US) are selected to evaluate the performance.
2. The performance of bidirectional architecture is analysed for bidirectional signals under fiber nonlinearities, VLC channel noise and free-space clear with weak turbulent conditions.
3. For both FSO and red LED based VLC system line of sight is utilized because it assisting in acquiring maximal speed, large bandwidth as well as minimum link interference with least signals loss.

3.1. FSO atmospheric losses

FSO link comprises major impairments such as different climate conditions, turbulent effects, pointing error and geometric losses. In general, FSO link gain, c comprises mainly path-loss c_l, pointing errors, c_p and atmospheric turbulence, c_a. Mathematically, FSO link gain is given as [22]:

$$c = c_a c_p \, c_l \tag{5}$$

The received power, P_{re} in FSO link under distinct climate conditions can be defined as [23]:

$$P_{re} = P_{tr}.\left(\frac{A_{eff}}{(\theta L)^2}\right).exp\left(-\delta L_{fso}\right) \tag{6}$$

where P_{tr} is transmitted power. A_{eff} is antenna effective aperture area at Rx, θ is beam divergence, L is transmission distance and δ is attenuation coefficient depending on snow atmospheric conditions. Again, path-loss as per Beer-Lambert law is presented as [24]:

$$c_l = exp\left(-\delta L_{fso}\right) \tag{7}$$

In FSO the atmospheric turbulence effects introduce amplitude and phase variation of the propagating light, which causes fading as well as pulse abnormality. The strength of atmospheric turbulence as respects refraction structure parameter,C_n^2 is measured as [25]:

$$C_n^2 = (79 \times 10^{-6}.AX^{-2})^2 C_T^2 \tag{8}$$

where A exhibits atmospheric pressure, X is average temperature and C_T^2 is temperature structure parameter. Gamma-Gamma FSO distribution model generally used to realize the system performance because of its superb fitness over wide range turbulent effects from weak to strong as compared to others models. Therefore, proposed architecture having GG channel distribution in FSO link is defined as [25]:

$$f_{c_a}(c_a) = \frac{2(jk)^{\left(\frac{j+k}{2}\right)}}{\Gamma(j)\Gamma(k)}.h_a^{\left(\frac{j+k}{2}\right)-1}H_{j-k}\left[2(jkc_a)^{\frac{1}{2}}\right] \tag{9}$$

where $\Gamma(\cdot)$ is Gamma function, H_{j-k} is modified Bessel function, $(j-k)$ is Bessel function order, j and k are number of large & small scale irradiance fluctuations (effective eddies) are described as [25]:

$$j = \left\{\left[(0.49k_0^2).\left(1+0.18d^2+0.56k_0^{\frac{12}{5}}\right)^{-7/6}\right]-1\right\}^{-1} \tag{10}$$

and

$$k = \left\{\left[\frac{0.51k_0^2\left(1+0.18d^2+0.56k_0^{\frac{12}{5}}\right)^{\frac{-5}{6}}}{\left(1+0.90d^2+0.62d^2k_0^{\frac{12}{5}}\right)^{\frac{5}{6}}}\right]-1\right\}^{-1} \tag{11}$$

where d is spherical wave diameter and k_0 is aperture-averaged of atmospheric fading strength. Furthermore, Mathematically, BER of the proposed design concerning FSO GG fading model and m-QAM OFDM-VLC is evaluated as [25]:

$$BER = \frac{2}{log_2(m)}\left(1-\frac{1}{\sqrt{m}}\right)erfc$$

$$\left(\sqrt{\frac{3}{2(m-1)}\times\frac{1}{EVM^2}}\right)+$$

$$\frac{1}{2}\int_0^{\infty} f_{c_a}(c_a)\, erfc\left(\frac{\langle SNR\rangle s}{2\sqrt{2}\langle i_s\rangle}\right) ds \qquad (12)$$

where $erfc(.)$ depicts complementary error function, m is level of modulation format, EVM means error vector magnitude, h_a means atmospheric turbulence, $\langle SNR\rangle$ mean signal to noise ratio, s is signal strength and i_s is signal current at photo-detector.

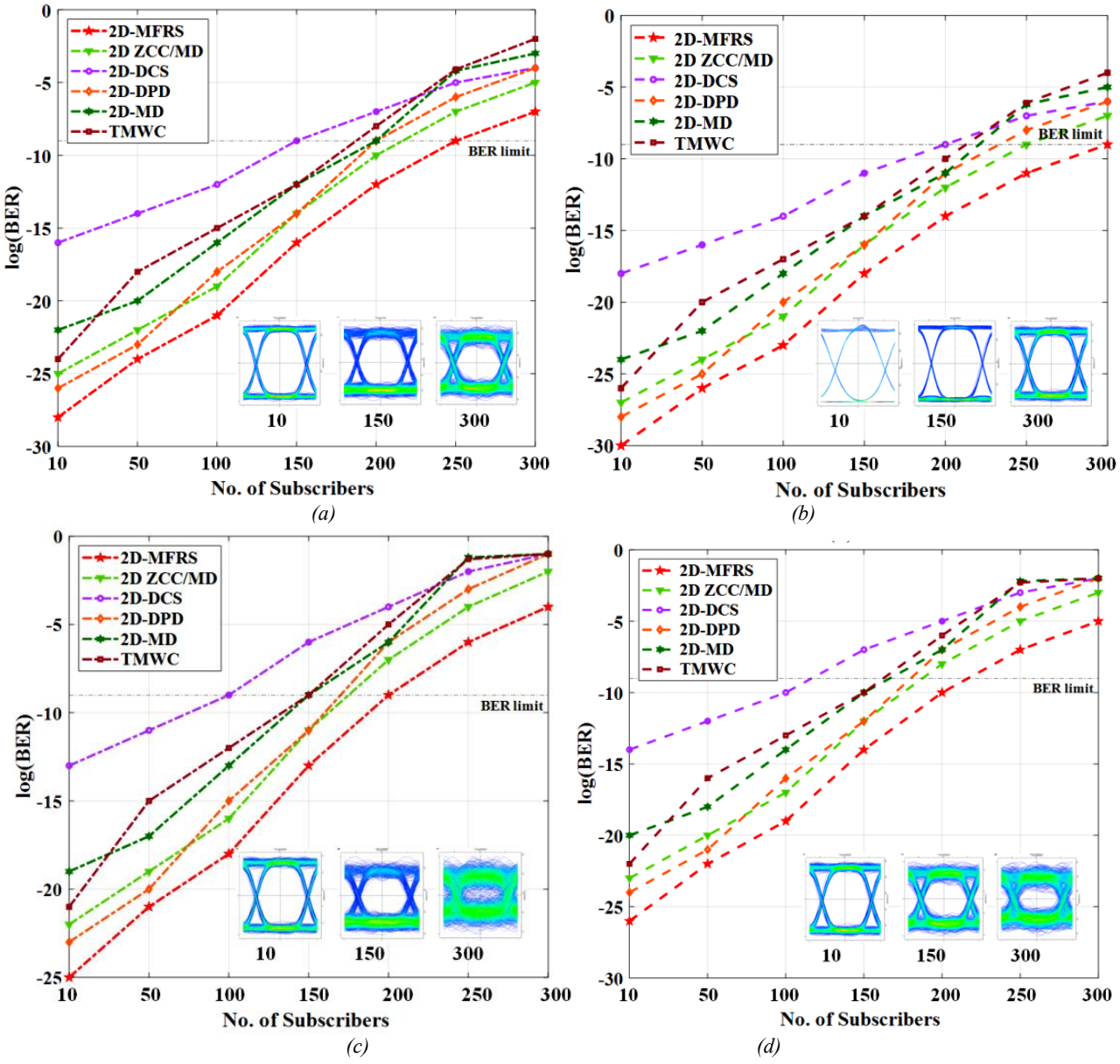

Fig. 4. System BER for distinct subscribers of different codes at (a) 50Gbps in DS, (b) 50Gbps in US, (c) 100Gbps in DS and (d) 100Gbps in US. Insets: corresponding eye diagrams for 2D-MFRS code (colour online)

Besides this, with an increase in throughput from 50Gbps to 100Gbps, especially worsen the system BER. This is due to the brought-up noise level in channels that substantially diminish the system's performance and thus channel traffic rate will be hugely decreased. Indeed, 2D-MFRS performs superior over other codes supporting 250 and 350 subscribers in DS and US transmission respectively, at 50Gbps transmission rate under BER limit as described in Fig. 4(a) and 4(b). However, when the channel rate increases from 50 to 100Gbps, the no. of supporting subscribers deteriorates to 200 in DS and 210 in US direction as noted in Fig. 4(c) and 4(d).

Moreover, Fig. 4(a)-4(d) indicates the corresponding eye diagrams for 10, 150 and 300 subscribers at 50 and 100Gbps transmission rates. As anticipated, whenever the no. of working subscribers improves, the signal begins to fade as can be ascertained in eye patterns along with BER. It is perceived that required output with open as well as wide eye patterns is attained for fewer no. of subscribers in DS/US transmission [26]. Again, Table 3 indicates the

maximum no. of subscribers supported by them system using different codes at 50 and 100Gbps transmission rate. It is certain that 2D-MFRS can supports maximum end subscribers; 2D-MD/ZCC code performs best followed by other 2D codes like MD/ZCC, DPD, MD, DCS and even TWWC codes in both DS and US at varied transmission rate.

Table 3. Maximum no. of supportable subscribers @log(BER) of -9

Code/dimension	50Gbps		100Gbps	
	D/S	U/S	D/S	U/S
MFRS/2D	250	300	200	210
Multi-diagonal/zero cross-correlation (MD/ZCC)/2D	210	250	170	190
Diluted perfect difference (DPD)/2D	200	230	160	180
MD/2D	200	220	150	160
Transposed modified walsh code (TMWC)/1D	190	210	150	160
Dynamic cyclic shift (DCS)/2D	150	200	100	110

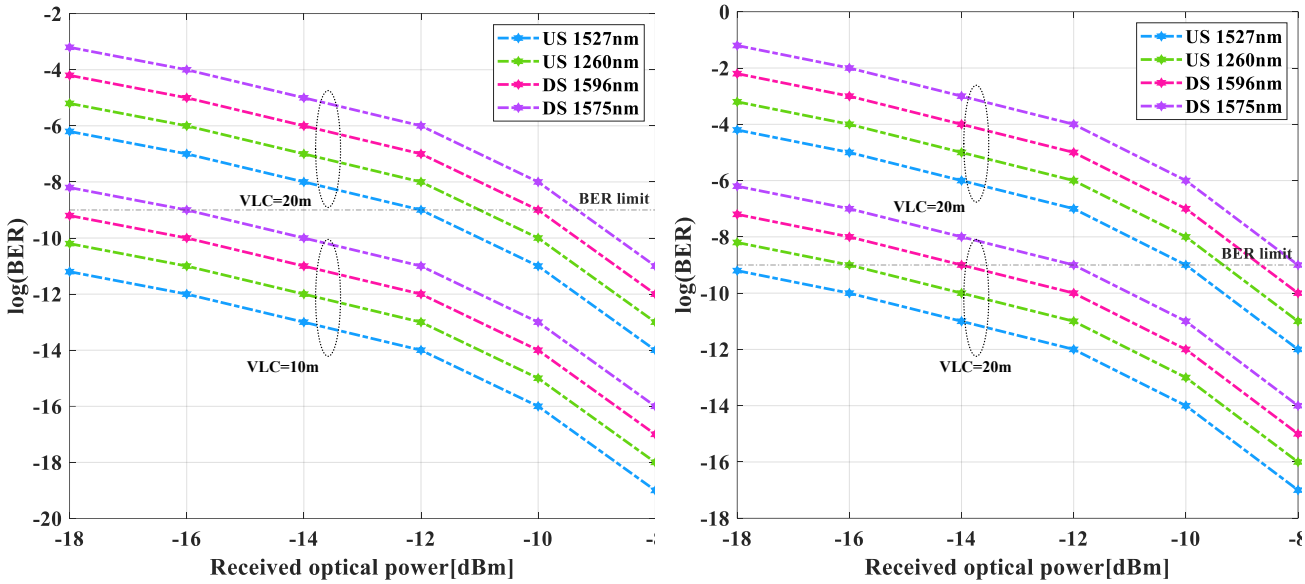

Fig. 5 Measured BER for different DS/US wavelengths over 10 and 20m VLC range of the system supporting (a) 10 ONUs/RNs and (b) 20 ONUs/RN (colour online)

Fig. 5(a) and (b) illustrates the measured BER as a consequence of receiver power in each channel in DS/US direction for system supporting 10 and 20 ONUs/RN respectively, at fixed 50km fiber+100m FSO range having 40/40Gbps throughput. The system performance is evaluated for two DS (1596 and 1575nm) and two US (1527 and 1260nm) wavelength signals for varied VLC range of 10 and 20m. It is depicted that system supporting lower number of ONUs/RN provides best performance for various signals at varied VLC range. As shown in Fig. 5(a), the receiver sensitivities of -18 to -16dBm over 10m VLC and -12 to -9dBm over 20m VLC range is observed for various transmission wavelengths, at BER limit. Also, for the same transmission, receiver sensitivities of -18 to -12dBm and -10 to -8dBm over 10 and 20m VLC range is achieved respectively. BER with minor sensitivity confirms the feasibility of designed system, as in Fig. 5(b). Table 4 indicate the obtained minimum received power values for different wavelengths at 10 and 20m VLC ranges.

Table 4. Obtained minimum received power values for different wavelengths at varied VLC range @log(BER)=-9

No. of ONUs/RN	ROP(dBm)			
	10	20	10	20
Wavelengths (nm)	VLC=10m		VLC=20m	
1596	-18	-10	-14	-8.5
1575	-16	-9	-12	-8
1527	<-18	-12	<-18	-10
1260	<-18	-11	-18	-9.5

Fig. 7(a-f) depicts the obtained spectra of 2D-MFRS code at different fiber ranges which illustrate the distorted time domain achieved for code with the increase in range at receiver side.

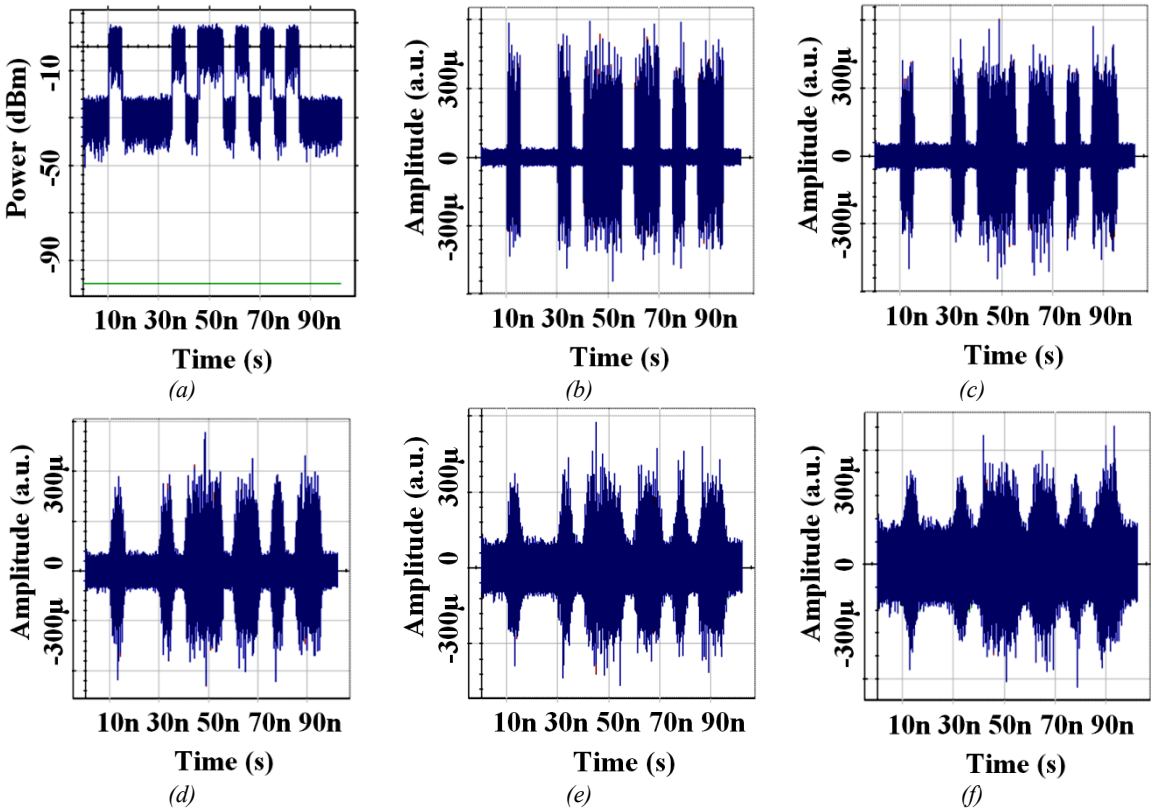

Fig. 7. Obtained time domain spectra of 2D-MFRS code at (a) 10km and (b) 20km, (c) 30km (d) 40km, (e) 50km, (f) 60km SMF range (colour online)

From Fig. 7(a) it is clear that the time domain spectra of 2D-MFRS code results in distorted with increase in transmission range. It is because of presence of fiber impairments, severe atmospheric conditions in FSO and background, thermal and shot noise in VLC link. Due to all these effects, 10dBm power obtained at 10km reduces a thus the pattern of the code distorted with the increase in range upto 60km SMF with fixed 100m FSO and 10m VLC range in the proposed system.

The system comparisons with exiting works are shown in Table 5. It is clear that out of existing works, this design offers maximum integrated wired-wireless range by considering both simulation in [27–29] and experimental investigation in [30–34]. Meanwhile, the key outcomes of this work are given as:

- Maximum fiber distance of 50km with fronthaul 100m FSO and 20m VLC range is achieved.
- The proposed architecture can support upto 300 ONUs at 10×100Gbps data rate while maintain receiver sensitivity of -10dBm.
- Compared to other OCDMA codes, 2D-MFRS code can offers maximum transmission distance, data rate and high capacity.

In short, to minimise the effects of a failure, the wheel topology will route data from the broken or failed path onto an alternative linked path that primarily surrounds the OLT channel or a nearby RN or ONU. Briefly, in this architecture, all remote and end nodes are separated from hospital management via rocky ground, river or mountain concerning clouds, rain, snow, fog, dust, direct sun light, moving objects and weak-to-strong turbulent [11]. In these scenarios, wheel-POLAN healthcare system for disaster preparedness provides most preferable solution to make end nodes connectively for providing medical services.

Table 5. Comparison of various PON based designs based on topology

System	Year	Transmission	Topology	SMF range (km)	Wireless range (m)	No. of channels	Throughput /channel (Gbps)	Cost	Complexity	Applications	Realization
WDM [27]	2018	Simplex	Integrated ring-tree	100	-	-	60	Moderate	High	High capacity network	Simulation
Hybrid TDM-WDM [32]	2021	Duplex	Hybrid ring-tree	26	-	-	1.25	High	High	Fiber breakpoint avoidance	Experimental
PON-FSO [28]	2023	Duplex	Hybrid ring-mesh	130	1900	10	10	High	High	5G fronthaul/backhaul	Simulation
PON [29]	2024	Duplex	Wheel	310	-	8	50	Moderate	High	5G backhaul	Simulation
PON-FSO [This work]		Duplex	Wheel	50	100 (FSO)+ 20 (VLC)	10	100	Moderate	Medium	High-speed, secure and long reach flexible healthcare systems	Simulation

4. Conclusion

A wheel POLAN architecture basics 10×100Gbps OCDMA PON using 4-QAM OFDM scheme for geographical disaster failures in healthcare services is designed and investigated. 2D-MFRS code is used in the proposed system over FSO-VLC links for end-user connectivity. It is concluded that faithful fiber distance can be obtained upto 50km with fronthaul 100m FSO and 20m VLC links. Proposed wheel-based architecture supporting 20 ONUs per remote node is maintain the minimum receiver sensitivity of -10dBm over hybrid 50km fiber-100m FSO and 20m VLC range. Also, the large number 200 to 300 end subscribers can be served by the proposed model having 2D-MFRS code upto 100Gbps transmission rate as compared to other codes. In addition, the comparison of proposed architecture in terms of codes and topology design indicates reliable long-reach, feasible high bit rate, secure data for several subscribers in cost effective manner for healthcare applications. However, the proposed design incorporates few challenges like multiuser interference, heterogeneous channel impairments, synchronization issues etc. It should be ensured that reliable high-capacity communication across integrated fiber-FSO-VLC link and atmospheric require optimized as well as robust resource allocation. In future, this architecture can be incorporated to provide high capacity, radiation-free as well as secure outstanding features in healthcare systems supporting various indoor/outdoor hospital scenarios to encourage several medical assessment research communities for the improvement of people's health.

References

[1] S. M. Jung, K. H. Mun, S. M. Kang, S. K. Han, Optical Fiber Technology **45**, 289 (2018).
[2] S. Bindhaiq, N. Zulkifli, A. M. Supa, Optical Fiber Technology **30**, 65 (2016).
[3] Y. Nakayama, R. Yasunaga, Wireless Networks **27**, 3635 (2021).
[4] M. Chen, H. Lu, D. Chen, J. Jin, J. Wang, Optics Communications **473**, 125993 (2020).
[5] H. Li, Y. Zhang, X. Chen, C. Wu, J. Guo, Z. Gao, W. Pei, H. Chen, Optics Communications **354**, 107 (2015).
[6] M. Lu, S. Xiao, L. Zhang, L. Zheng, J. Fang, T. Huang, W. Hu, Optics Communications **452**, 252 (2019).
[7] R. Deng, J. He, M. Chen, Y. Zhou, Optics Communications **423**, 69 (2018).
[8] C. W. Chow, C. H. Yeh, Y. F. Liu, P. Y. Huang,

Y. Liu, Optics Communications **292**, 49 (2013).
[9] J. Zhang, X. Hong, J. Liu, C. Guo, Optics Communications **412**, 219 (2018).
[10] X. Li, C. Min, S. Gao, Y. Wang, X. Chen, H. Chen, Optics Communications **453**, 124420 (2019).
[11] A. Zentani, N. Zulkifli, A. Ramli, Optical Fiber Technology **73**, 103038 (2022).
[12] P. Roychowdhury, J. M. Alghazo, G. Latif, Wireless Networks **27**, 781 (2021).
[13] C. H. Yeh, F.-Y. Shih, G.-K. Chang, S. Chi, Optics Express **16**, 4494 (2008).
[14] K. Mallick, P. Mandal, B. Dutta, B. Kuiri, S. Santra, R. Mukherjee, A. S. Patra, IEEE Photonics Journal **13**, 1 (2021).
[15] P. Mandal, K. Mallick, S. Santra, B. Kuiri, B. Dutta, Optical and Quantum Electronics **53**, 1 (2021).
[16] N. Sarkar, S. Banerjee, P. Mandal, P. Tudu, Optical and Quantum Electronics **54**, 1 (2022).
[17] Z. Q. Zhong, W. Jin, S. Jiang, J. X. He, D. Chang, Y. H. Hong, R. P. Giddings, X. Q. Jin, M. Oasullivan, T. Durrant, J. Trewern, G. Mariani, J. M. Tang, Journal of Lightwave Technology **39**, 7360 (2021).
[18] A. Adnan, Y. Liu, C. W. Chow, C. H. Yeh, Optics Communications **472**, 125991 (2020).
[19] C. H. Yeh, W. H. Hsu, B. Y. Wang, W. Y. You, J. R. Chen, C. W. Chow, S. K. Liaw, IEEE Access **8**, 189982 (2020).
[20] M. Kumari, A. Sheetal, R. Sharma, Wireless Personal Communications **119**, 2539 (2021).
[21] H. Yousif Ahmed, M. Zeghid, W. A.Imtiaz, Y. Sharief, A. Sghaier, Optik **185**, 746 (2019).
[22] M. Kumari, S. K. Mishra, Micromachines **16**, 1 (2025).
[23] M. Kumari, Internet Technology Letters **8**, e70023 (2025).
[24] M. Kumari, Journal of Optical Communications **46**, 347 (2024).
[25] M. Kumari, Optoelectron. Adv. Mat. **18**(3-4), 150 (2024).
[26] A. Shahpari, R. Ferreira, V. Ribeiro, A. Sousa, S. Ziaie, A. Tavares, Z. Vujicic, F. P. Guiomar, J. D. Reis, A. N. Pinto, A. Teixeira, Optical Fiber Technology **26**, 100 (2015).
[27] Sukhbir Singh, Surinder Singh, Photonic Network Communications **35**, 325 (2018).
[28] M. Kumari, Optical and Quantum Electronics **55**, 1098 (2023).
[29] M. Kumari, Journal of Ambient Intelligence and Humanized Computing **15**, 2439 (2024).
[30] P. J. Winzer, A. H. Gnauck, C. R. Doerr, M. Magarini, L. L. Buhl, Journal of Lightwave Technology **28**, 547 (2010).
[31] S. Zhu, P. Qiu, X. Shan, Z. Wang, R. Lin, X. Cui, G. Zhang, P. Tian, IEEE Photonics Journal **14**, 1 (2022).
[32] C. Y. Li, C. H. Chang, Z. G. Lin, Photonics **8**, 515 (2021).
[33] M. Zhang, Y. Li, S. Wei, H. Song, Y. Wang, Y. Zhao, J. Zhang, IEEE Photonics Technology Letters **37**, 141 (2024).
[34] C. Hu, G. Wang, Z. Fan, J. Zhao, Journal of Lightwave Technology **41**, 5622 (2023).

*Corresponding author: ichvivekmalik@gmail.com